Journal of The Electrochemical Society, **160** (6) C197-C205 (2013)
0013-4651/2013/160(6)/C197/9/$31.00 © The Electrochemical Society

Oxide Film Growth Kinetics on Metals and Alloys

II. Numerical Simulation of Transient Behavior

Kirsten Leistner,[a] Charles Toulemonde,[b] Boubakar Diawara,[a] Antoine Seyeux,[a] and Philippe Marcus[a,*,z]

[a]*Laboratoire de Physico-Chimie des Surfaces, CNRS (UMR 7045), Ecole Nationale Supérieure de Chimie de Paris (Chimie ParisTech), 75005 Paris, France*
[b]*EDF R&D Materials and Mechanics of Components Department, Site des Renardières, 77818 Moret sur Loing Cedex, France*

A number of passive film growth models have been advanced in the past, each founded on different assumptions and providing different rate laws. A new, generalized growth model has been developed and the numerical simulation of the transient behavior of oxide film growth on metals and alloys is reported here. This model is based on the transport of anions and cations (in a Cr_2O_3 film for stainless alloy). In contrast to most models up to date, it describes the time-variant behavior of film and film/solution potential differences. Because these potential differences are expressed as exponential functions of film thickness, asymptotic behaviors can be studied and it is shown that a square root law results for very thin and very thick films. Growth rate for intermediate films and during transient periods, on the other hand, is determined by numerical integration. Parameters which were introduced by the model and whose values are unknown are conveniently regrouped into only four lumped parameters, which are easily estimated by numerical optimisation. It is shown that experimental oxide film thickness measurements on stainless alloys in high-temperature aqueous environments can be reproduced. It is further shown that the diffusional rate expressions of all the species contributing to growth are analogous, explaining why it is possible to fit growth kinetics with a single type of point defect.
 [DOI: 10.1149/2.037306jes]

Manuscript submitted January 14, 2013; revised manuscript received February 19, 2013. Published March 12, 2013.

Most metals exposed to air and other oxidizing environments gradually corrode. However, many metals exhibit protective corrosion behavior because they form an inert oxide layer which isolates them from the surrounding environment, effectively limiting further deterioration. This behavior, which is known as passivity,[1,2] is of major importance in a number of industries, including the chemical industry and high-temperature installations such as nuclear power plants. Prediction and understanding of passivity is crucial and as a result, several film growth models have been published, starting with Wagner in the nineteen thirties,[3] Mott[4] and Fehlner and Mott.[5] In the nineteen eighties, a model called the Point Defect Model (PDM) was published by Chao et al.[6] Most of these models deal with oxide layers on pure metals rather than alloys. More recently two additional models describing the growth of oxide films on alloys have been published: the mixed conduction model[7,8] and an atomistic model

A thorough review of published models has been made in Part One of this study,[9] and by and large, film growth laws have been shown to be of one of three types,

$$x = A + B \ln t \text{ (logarithmic law [5, 6])} \quad [1]$$

$$\frac{1}{x} = C - D \ln t \text{ (inverse logarithmic law [10, 11])} \quad [2]$$

$$x^2 = E \cdot t \text{ (parabolic law [3, 6, 10, 11])} \quad [3]$$

where x is the film thickness and A, B, C and D are constants with respect to time t. Any attempt at modeling oxide layer growth must be based on a number of hypotheses, concerning, amongst others, the nature of the chemical species responsible for growth, strength and behavior of the electric field and potential drop in the film. For instance, having originally been developed for oxidation of metals in air, the Wagner and Mott-Cabrera growth models take into account neither the potential drop at the film-solution interface nor solution pH.[3,4,10,11] Mott and Cabrera also assume that only cation diffusion via interstitial sites brings about film growth when the rate is controlled by species transport and that the metal/oxide reaction is rate determining under strong electric fields. The later Fehlner-Mott model on the other hand, attributes growth to interstitial anion diffusion and, like the earlier models, neglects potential drops at both metal/film and film/solution interfaces.[5] Macdonald's PDM takes these potential drops into account, but attributes growth to oxygen (anionic) vacancies.[6] Later extensions describe cases where reactions at the interfaces become rate determining and include film dissolution.[12,13] In all of the above-mentioned models, electric field strength is assumed constant throughout the film. Note also that all of these models are applicable to pure metals rather than alloys since the presence of more than one cationic species is never considered. If one considers the number and diversity of all these hypotheses, it is not surprising that no unique growth law has been identified.

Part One of this study introduced a new model for oxide film growth on alloys.[9] It is closely related to the previous models, including the PDM,[6] in that the rate determining step is taken to be diffusion of point defects across the oxide layer and in that the diffusional rate is determined from Fick's Law where interfacial concentrations for the steady state are calculated from electrochemical equilibria. The PDM does not consider the non-steady state, but the new model does. It computes non-steady state concentrations by using transient potential drops in the same formula used for the steady state. Also similarly to the PDM,[6] the potential difference between metal and solution is partitioned between the metal/film interface, the film itself and the film/solution interface and film dissolution limits growth. However, unlike most models in the literature, this generalized model is derived without making one of the most common hypotheses, that of an electric field constant in time. It also does not assume that only a single species is responsible for growth, but rather supposes that oxygen vacancies, cation vacancies in lattice positions and cations in interstitial positions all contribute. As an example, it describes the growth of passive films on stainless alloys and takes into account their composition and the contribution of each of the components. Nevertheless, because of its generality, the new model contains numerous parameters that are difficult or even impossible to determine directly by experiment, including Gibbs free energies of the interfacial reactions, diffusion coefficients of point defects and potential drops at the interfaces. Thus, the task of the present study is also to investigate the possibility of determining such parameters numerically.

In this study, we start off from the model described in Part One.[9] First, the main features of this model are summarized and some details are given concerning the electrical field in the oxide and how its behavior impacts the film growth rate law. We then go on to show that the defining differential equation can be solved using a Runge-Kutta type method. As an illustration, parameters in the model are estimated

*Electrochemical Society Fellow.
[z]E-mail: philippe-marcus@chimie-paristech.fr

by numerical optimisation against experimental data relevant to the primary side of pressurized water reactors (PWRs), i.e., Alloy 600 or 690 or 304 stainless steel in contact with high temperature water (~300 °C). We further show that, from the general formulation, a simplified model may be derived, resulting in a reduced number of lumped parameters. This reduced model is shown to be preferable for the purpose of obtaining physically significant parameter values.

Model

Generalized model for oxide film growth.— The generalized model for film growth was first presented in Part One of this study.[9] In this section, the main hypotheses and results of this previous study are summarized, for more detail see.[9] In brief, the model supposes that species transport across the film is the rate determining step for film growth on alloys under most conditions. Interfacial reactions are rate determining only for very thin films. In this study only rate control by species transport will be considered. Three species, oxygen vacancies, Cr cations in lattice positions and Cr cations in interstitial positions, contribute to the growth process. All other cations (Fe, Ni) are released into the solution and the film is made up of Cr_2O_3 only. The growth law, derived from a generalized form of Fick's First Law applied to each species j, is:

$$\frac{dx}{dt} = \frac{\Omega}{N_v}[J_{V_{\ddot{O}}} + J_{M_{Cr}} + J_{I_{Cr}}]$$

$$= \frac{\Omega}{N_v}\sum_j \left[\frac{q_j F D_j \phi_f(x)}{RTx} \cdot \frac{C_i\,|_{m/f}\,\exp\left[\frac{q_j F \phi_f(x)}{RT}\right] - C_j\,|_{f/s}}{\exp\left[\frac{q_j F \phi_f(x)}{RT}\right] - 1}\right], \quad [4]$$

where the sum is taken over $j \in [V_{\ddot{O}}, M_{Cr}, I_{Cr}]$ and m/f and f/s denote the alloy/film and film/solution interfaces, respectively. Film thickness is represented by the symbol x, J_j is the flux of species j in number of species per m^2 per second, q_j and D_j are the charge and the diffusivity of species j, respectively and C_j its concentration. The concentrations of species j at a given interface can be determined following a procedure already outlined by Chao et al.[6] and are given in.[9] The species considered are oxygen vacancies, $V_{\ddot{O}}$, metallic cations (Cr, Fe or Ni) in cation positions, M_{Cr} and cations in interstitial positions, I_{Cr}. F is the Faraday constant, R the universal gas constant, T the temperature in Kelvin, Ω the molar volume of the oxide in m^3/mol and N_V Avogadro's number.

A potential drop exists at the interface of an oxide-covered alloy exposed to water. It acts as a driving force, giving rise to diffusion of the above-mentioned species, which in turn causes the oxide film on the alloy surface to grow. The potential difference V between alloy and solution is commonly held to be the sum of the three individual potential drops: $V = \phi_{m/f} + \phi_f + \phi_{f/s}$.[14] All previous growth kinetics models, if indeed they acknowledge this distribution of potentials at all, assume that each of these potential drops is constant during growth, and thus independent of thickness x; in other words, they only consider steady state behavior. This is probably partly owing to the fact that some existing models were conceived for comparison with potentiostatic experiments.[15,16] For instance, the first to explicitly divide the overall potential drop into the above-mentioned three contributions is the PDM,[6] but it does not consider them to be functions of film thickness x and therefore of time (though it does see them as functions of solution pH and applied potential). Nevertheless, time-variance of defect concentration in the film has been accounted for by Bojinov.[7,17] Note that some of the earlier models consider the total potential drop to be constant, and accordingly, that electric field strength changes with x. More generally however, when the system is subjected to a change in potential difference ΔV, occurring, for instance, when the chemistry of the solution or the temperature changes, a transient period ensues. During this period, the potential differences and the electric field in the film can be presumed to evolve with x, until the latter reaches a new steady state value x_f.

Our hypothesis for the generalized model is that the potential across the film is a linear function of position, d. This assumption holds for both transient and steady states, but the gradient of the linear function will evolve during the transient. From this assumption it follows that the electric field strength F is constant throughout the film because $F = \partial\varphi_f/\partial d$. Fick's law is also simplified by the assumption that the concentration throughout the film is a linear function of the position, d. This assumption allows one to derive Equation 4. The hypothesis on the concentration profile is likely to be justified in the middle of the film, but border effects are neglected.

Given the hypothesis on the potential drop across the film, the electric field in the film is constant at steady state, but varies under non-steady state (transient) conditions until it returns to its original value once steady state is reached. This behavior can be seen in Figure 1a by observing that the slope $\partial\phi_f/\partial d$ is time-variant at first, but always assumes the same value at steady state. Note that the electric field is presumed to be independent of position within the film at all times, hence the linearity of ϕ_f. According to Equation 4 the system responds to the change in potential difference. At the initial moment, it is distributed over the interfaces and the film in the following manner: $\Delta V = \Delta\phi_{m/f}(x_i) + \Delta\phi_f(x_i) + \Delta\phi_{f/s}(x_i)$, where x_i is the initial film thickness. The modified potential differences cause species fluxes and thus film growth rate to evolve. The transient behavior, which can be observed in Figure 1b, is expressed in

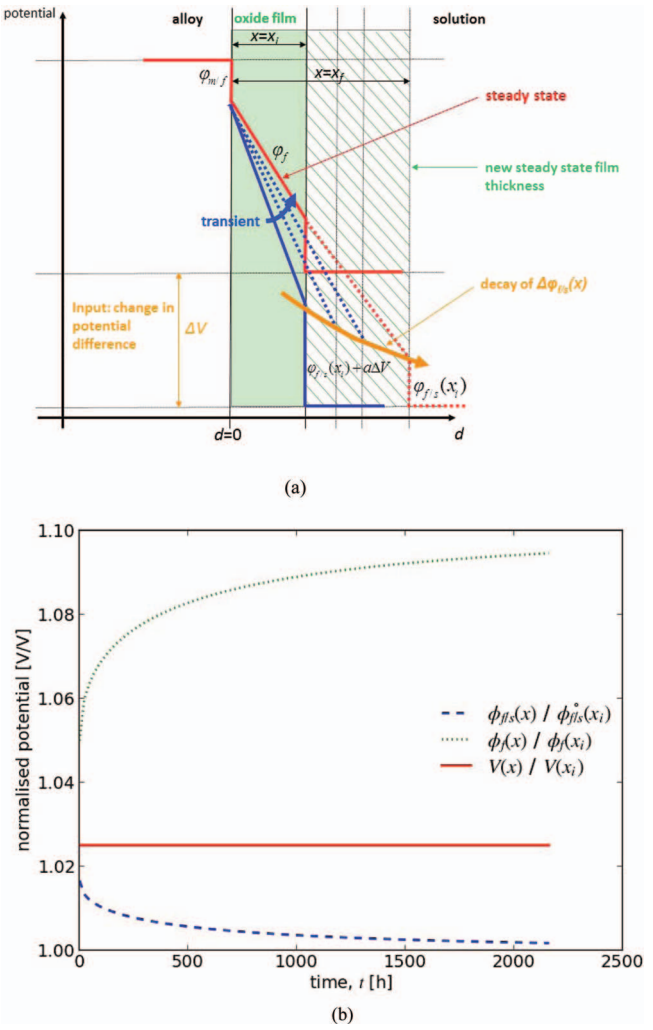

Figure 1. Temporal evolution of ϕ_f, $\phi_{f/s}$ and V during oxide film growth.

Equations 5–7.

$$\phi_{m/f}(x) = \phi^{\circ}_{m/f}(x_i) = const \quad [5]$$

$$\phi_{f/s}(x) = \phi^{\circ}_{f/s}(x_i) + \Delta\phi_{f/s}(x) = \phi^{\circ}_{f/s}(x_i) + \alpha\Delta V e^{-x/x_d} \quad [6]$$

$$\phi_f(x) = \phi_f(x_i) + \Delta\phi_f(x) = \phi_f(x_i) + \Delta V(1 - \alpha e^{-x/x_d}). \quad [7]$$

In Equation 5, the structure of the m/f interface and alloy composition are assumed constant during film growth. In these conditions $\phi_{m/f}$ is constant and equal to the equilibrium potential at that interface. As Figure 1b shows, $\phi_{f/s}(x)$ decays from its initial value of $\phi^{\circ}_{f/s}(x_i) + \Delta\phi_{f/s}(x_i)$ until, at steady state, it again assumes its original (equilibrium) value, $\phi^{\circ}_{f/s}(x_i)$. This decay was described in Part One[9] by a generic decreasing function, $f(x)$ fulfilling the condition $f(x_f) = 0 \leq f(x) \leq f(x_i)$. It is assumed[9] that the decay is exponential, hence the term e^{-x/x_d} in Equation 6, in which the decay length x_d is characteristic of a given metal-film-solution system and indicative of the film thickness necessary for ΔV to decay. It is in fact a reference length that allows the model to judge the order of magnitude of a given x as small, large or intermediate and satisfy the above-mentioned condition: $f(x_f) = 0$ if $x_f \gg x_d$ and $f(x_i) = 1$ if $x_i \ll x_d$.

Equation 7 shows that the behavior of $\phi_f(x)$ is the inverse of that of $\phi_{f/s}(x)$. As the film grows, ϕ_f also grows until it reaches a new steady state value. The constant α is the fraction of the overall change, ΔV, that is apportioned to $\Delta\phi_{f/s}(x_i)$. Similarly, $(1 - \alpha)$ is the fraction allotted to $\Delta\phi_f(x_i)$. If $\alpha = 0$, $\phi_{f/s}(x)$ would not undergo any variation and only $\phi_f(x)$ would evolve during the transient period. Note that the steady state mentioned in the above discussion refers to a situation of time-invariant electric field, where dx/dt is constant, not to the pseudo-steady state reached when dissolution equals growth rate and $dx/dt = 0$.

Numerical solution and parameter estimation.— In the general case (intermediate values of x), the differential equation 4 must be solved numerically. It was integrated according to a second order Runge-Kutta type algorithm:

$$\frac{dx}{dt} = f(x)$$
$$x_{t+1} = x_t + h\left(f(x_{t+1/2})\right),$$

where h is the integration step and $x_{t+1/2} = x_t + \frac{h \cdot f(x_t)}{2}$. Occasionally $f(x)$ is a very steep function of x, in fact, solution of Equation 4 shows that species fluxes are exponential functions of x (see simulations in later sections, e.g. Figure 8). In such cases, the above integration scheme has to be corrected, otherwise it may result in $x_{t+1/2} > x_{t+1}$. Under these conditions, $x_{t+1/2}$ is recalculated according to $x_{t+1/2} = (x_t + h \cdot f(x_{t+1/2}))/2$. Coding was done in C for integration into EDF's Materials Aging Platform (MAP).[18] Parameters were pre-estimated by manual fitting and then optimized by coupling the code to the ADAO optimisation module of EDF's SALOME platform.[19] The three-dimensional variational (3DVAR) algorithm was used, and for better scaling, the logarithm of some parameters, in particular of diffusivities, was optimized.

Results and Discussion

Model simplification (anion vacancies) and asymptotic behavior.— In order to illustrate how the introduction of time-variant potential drops affects the behavior of the model, we first consider oxygen vacancy diffusion, neglecting other species fluxes for the time being. Equation 4 becomes

$$\frac{dx}{dt} = \frac{\Omega}{N_V} J_{V_{\ddot{O}}} \quad [8]$$

Substituting the concentrations from Figure 6 of Part One,[9] one then obtains

$$\frac{dx}{dt} = \frac{\mathrm{F} q_{V_{\ddot{O}}} D_{V_{\ddot{O}}} \phi_f(x)}{RTx} \cdot \frac{\exp\left[\frac{-2/3\Delta G^{\circ}_1 + 2\mathrm{F}\phi_{m/f}}{RT} + \frac{2}{3} ln\chi_{Cr}\right] \exp\left[\frac{q_{V_{\ddot{O}}}\mathrm{F}\phi_f(x)}{RT}\right] - \exp\left[\frac{\Delta G^{\circ}_8 - 2\mathrm{F}\phi_{f/s}(x)}{RT} - 4.606 \cdot pH\right]}{\exp\left[\frac{q_{V_{\ddot{O}}}\mathrm{F}\phi_f(x)}{RT}\right] - 1} \quad [9]$$

Equation 9 may be further simplified by factoring out $\exp[(\Delta G^{\circ}_8 - 2\mathrm{F}\phi_{f/s})/RT - 4.606 \cdot pH]$ to obtain

$$\frac{dx}{dt} = \frac{A(e^B e^C - 1)}{e^C - 1}, \quad [10]$$

where

$$A = \frac{\mathrm{F} q_{V_{\ddot{O}}} D_{V_{\ddot{O}}} \phi_f(x)}{RTx} \exp\left[\frac{\Delta G^{\circ}_8 - 2\mathrm{F}\phi_{f/s}(x)}{RT} - 4.606 \cdot pH\right]$$

$$B = \frac{-2/3\Delta G^{\circ}_1 + 2\mathrm{F}\phi_{m/f} - \Delta G^{\circ}_8 + 2\mathrm{F}\phi_{f/s}(x)}{RT} + \frac{2}{3} ln\chi_{Cr} + 4.606 \cdot pH$$

$$C = \frac{q_{V_{\ddot{O}}}\mathrm{F}\phi_f(x)}{RT}$$

As also shown by Chao et al.,[6] 1 may be negligible with respect to e^{B+C} when $e^{B+C} > 50$, $B + C > 4$ and thus, substituting Equations 5–7 for the $\phi(x)$,

$$\frac{-2/3\Delta G^{\circ}_1 + 2\mathrm{F}\phi^{\circ}_{m/f} - \Delta G^{\circ}_8 + 2\mathrm{F}\left(\phi^{\circ}_{f/s} + \alpha\Delta V e^{-x/x_d}\right)}{RT}$$

$$+\frac{2}{3} ln\chi_{Cr} + 4.606 \cdot pH + \frac{q_{V_{\ddot{O}}}\mathrm{F}\left(\phi_f + \left(1 - \alpha\Delta V e^{-x/x_d}\right)\right)}{RT} > 4$$

Substituting the values of the constants and the typical temperature of 600 K in the above expression, one obtains the following inequality:

$$1.93 \cdot 10^5 [V(d_i) + \Delta V] + 3326\, ln\chi_{Cr} + 22977\ pH > 19954 + \Delta G^{\circ}_{tot}$$

where $V(x_i) = (\phi^{\circ}_{m/f}(x_i) + \phi_f(x_i) + \phi^{\circ}_{f/s}(x_i))$ and $\Delta G^{\circ}_{tot} = 2/3\Delta G^{\circ}_1 + \Delta G^{\circ}_8$ is the free Gibbs energy of the reaction $\mathrm{R_{tot}} = \mathrm{R_1 R_8}$. If a worst case scenario is employed, one may eliminate some of the variables from the condition by using their most unfavorable values:

$\Delta V = 0$	valid in growth, not recession
$3326\, ln\chi_{Cr} = -7658$	taking as the lowest possible $\chi_{Cr} \sim 0.1$
$22977\,\mathrm{pH} = 0$	using pH = 0

Using these worst-case values shows that certainly $e^B e^C - 1 \sim e^B e^C$ if $1.93 \cdot 10^5 V(x_i) > 53210 + \Delta G^{\circ}_{tot}$. Similarly one can with certainty say that $e^C - 1 \sim e^C$ if $e^C > 50$, so that $C > 4$, hence $2 \cdot 9.65 \cdot 10^4 \left[\phi_f + \Delta V(1 - \alpha e^{-x/x_d})\right] > 19954$ and $\phi_f(x_i) > 0.1$ V. These two conditions cannot routinely be evaluated since $V(x_i)$ and $\phi_f(x_i)$ are not always measured. Nevertheless, ΔG°_{tot} is likely to be strongly negative, so that one can be almost certain of fulfilling the first condition. Besides, the use of worst-case values implies that fulfillment of the conditions certainly leads to similarity between the full and simplified model, whereas non-fulfillment does not necessarily mean that the two models are not similar. When carrying out a similar simplification, Chao et al. assume that two analogous conditions are

generally fulfilled[6] and in practice, when using relevant parameter values, we find that -1 is indeed negligible in both terms. In fact, more generally, one may rewrite Equation 10 as

$$\frac{dx}{dt} = \frac{q_j \mathrm{F} D_j \phi_f(x)}{RTx} C_j^{f/s} \frac{\frac{C_j^{m/f}}{C_j^{f/s}} e^C - 1}{e^C - 1}. \qquad [11]$$

For oxygen vacancies ($i = J_{V_{\ddot{O}}}$), the ratio $C_j^{m/f}/C_j^{f/s}$ is certainly ≥ 1, and so instead of fulfilling both above-mentioned conditions, it is only necessary to satisfy $e^C > 50$, i.e., $\phi_f(x_i) > 0.1$ V. If this condition is satisfied, e^C cancels out and Equation 10 becomes

$$\frac{dx}{dt} = Ae^B = K_1 \frac{[\phi_f(x_i) + \Delta V(1 - \alpha e^{-x/x_d})]}{x}, \qquad [12]$$

where

$$K_1 = \frac{q_{V_{\ddot{O}}} \mathrm{F} D_{V_{\ddot{O}}}}{RT} exp\left(\frac{-2/3\Delta G_1^\circ + 2\mathrm{F}\phi_{m/f}}{RT} + \frac{2}{3} ln \chi_{Cr}\right).$$

In general, Equation 12 cannot be integrated analytically, but some predictions can be made about its asymptotic behavior with the normalized film thickness, x/x_d.

For very small values of x/x_d, $e^{-x/x_d} \to 1$	For large values of x/x_d, $e^{-x/x_d} \to 0$
Thus Equation 12 becomes	Equation 12 becomes
$\frac{dx}{dt} = \frac{K_1[\phi_f(x_i) + \Delta V(1-\alpha)]}{x}$	$\frac{dx}{dt} = \frac{K_1[\phi_f(x_i) + \Delta V]}{x}$
$x(t) = \sqrt{K_1[\phi_f(x_i) + \Delta V(1-\alpha)]\, t}$	$x(t) = \sqrt{K_1[\phi_f(x_i) + \Delta V]\, t}$

We find that, for both very small and very large values of x/x_d, x grows with the square root of time; the two cases differ only by a constant, $\alpha\Delta V$, affecting the amplitude of the curve, as can be seen by comparing the solid and dotted curves in Figure 2. Note that the difference between the two cases becomes negligible when $\alpha \ll 1$, as then $x(t) = \sqrt{K_1[\phi_f(x_i) + \Delta V]\, t}$ for all x. But generally, intermediate values of x/x_d allow no simplification of the differential equation 12 and numerical integration is still necessary. However, the two limiting cases do show that this growth law behaves like two different square roots at the beginning of the experiment, for $t \sim 0$ (Figure 2a: the dashed curve overlaps with the dotted curve) and the end of the experiment, $t \to \infty$ (Figure 2b: the dashed curve tends to overlap with the solid curve). This also means that both very thin and very thick films grow according to square root laws. According to the generalized model, growth of films of intermediate thickness follows a more complex law. Note that in absence of any environmental change, $\Delta V = 0$ and in such conditions film growth will always proceed according to the square root $x(t) = \sqrt{K_1 \phi_f(x_i) t}$, independently of thickness.

It is interesting to observe that the PDM also predicts a parabolic rate of growth for very thin films (though not for very thick films).[6] Mott and Cabrera, on the other hand, do expect a parabolic growth law for very thick films, but not for thin ones[10,11] and Wagner's model always conforms to parabolic growth.[3] In the case of the PDM, the parabolic law for thin films is obtained by assuming potentiostatic conditions, i.e., constant potential differences and by truncating a series expansion of the rate law at the second order, while the growth law for thicker films is found by making some numerical simplifications. In the model presented in this study, whether a film is considered thick or thin will depend on the value of decay length x_d, which may therefore be presumed to represent a typical intermediate film thickness for a given system. This means that the model is general and will reproduce the above-mentioned behavior independently of the set experimental conditions.

Parameter optimisation and sensitivity analysis.— An attempt was made to estimate the optimisable parameters (i.e. all excluding T, χ_{Cr} and pH) by fitting $x(t)$ to the data for Alloy 690 exposed to water at 603 K.[20] The best fit obtained by the optimisation algorithm is shown in Figure 3a and the parameters in Table I. It appears that the model is not capable of reproducing the plateau which is approached at times after 1000 h. Simulations show that, even when the $\Delta\phi$ have reached steady state, $x(t)$ grows monotonically and growth rate dx/dt never equals 0. However, Figure 3b, in which the equations were fitted to the early points only, shows that the model does describe early film growth adequately. The parameter values used for this fit are the same as in Table I, except for $D_{V_{\ddot{O}}}$, which equals $5.3 \cdot 10^{-23}$ m^2/s here. It is expected that another term describing dissolution of the film is necessary to achieve a total growth rate of 0. However, some experiments do not exhibit a pseudo-steady state plateau and can therefore be modeled more accurately using an oxygen vacancy flux alone. Two such experiments are those of Tapping et al.[21] and Ziemniak et al.,[22] who measured film thickness as a function of time on type 304 austenitic stainless steel exposed to water at 573 and 533 K, respectively. These experiments were also simulated and the simulations shown in Figures 4 and 5, respectively. Note that the only difference between the fits to the three sets of experimental data is the value of $D_{V_{\ddot{O}}}$. It has similar values for the fits of Tapping's and Ziemniak's experiments ($8.0 \cdot 10^{-22}$ and $6.0 \cdot 10^{-22}$ m^2/s, respectively), but is more than an order of magnitude smaller for both fits to Carrette's data in

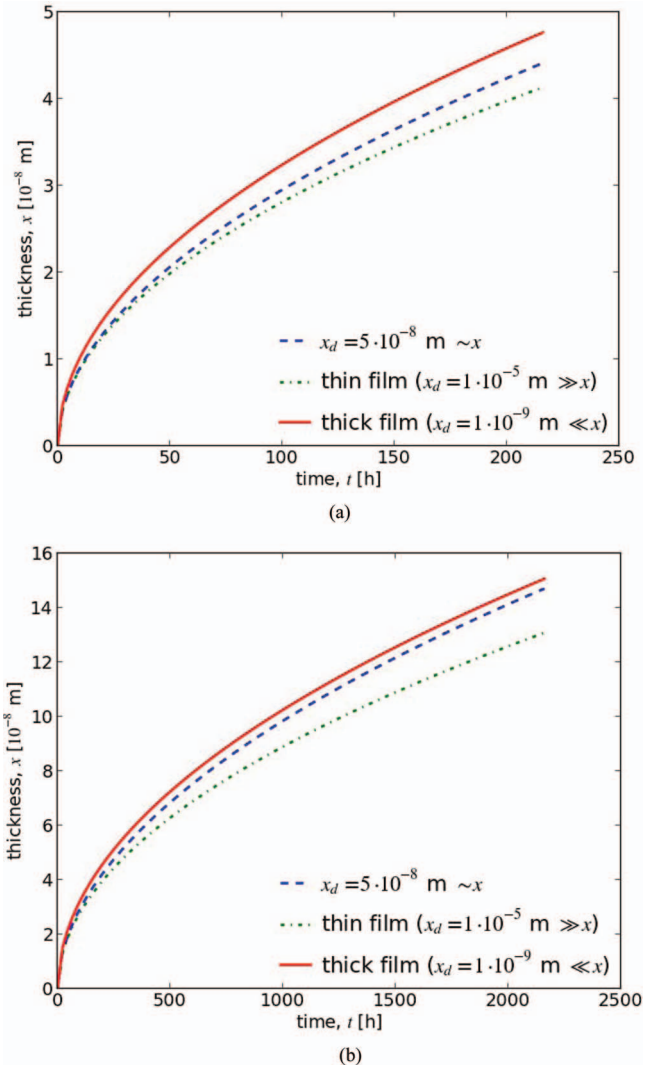

Figure 2. Asymptotic behavior of the model for thin and thick films. (a) For short growth times, the film behaves like a thin film, at intermediate times, the behavior deviates from the thin-film square root law. (b) For long growth times, the film behaves like a thick film (square root law).

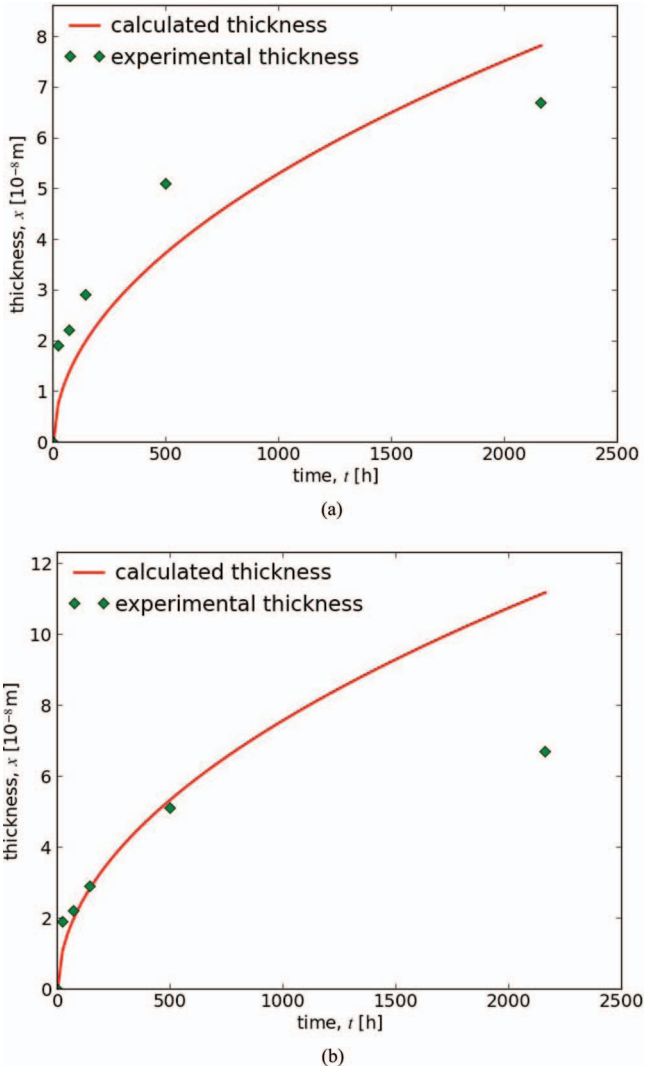

Figure 3. Calculated film thickness ($T = 603$ K, $pH = 7.2$ and $\chi_{Cr} = 0.32$) using optimized parameters and data for Alloy 690 in high temperature water.[20] (a) Fit to all points (b) Fit to early points only.

Figures 3a and 3b. Film thickness was measured by two different methods by Ziemniak et al. and thickness as predicted by the model fits in between the two.

Normalized sensitivity coefficients were calculated for each optimisable parameter A_k as $s_k(t) = A_k/x(t)\cdot\partial x(t)/\partial A_k$ in the simulations of Figure 3 and are shown in Figure 6a. Positive sensitivities indicate that an increase in the parameter will lead to an increase in x, whereas a negative s_j means that an increase in parameter A_k causes a decrease in x. It appears that ΔG_1° is the most sensitive parameter, followed by $D_{V_{\ddot{O}}}$ and $\phi_f(x_i)$. Note that the optimal value of $\phi_f(x_i)$ is 0.1 V, which satisfies the condition derived in the previous section. It is interesting to note that the sensitivities of ΔG_8° and $\phi_{f/s}^\circ(x_i)$ are zero, in support of the premise that $C_j^{f/s}$ can be canceled out in Equation 11; this means that concentration and potential at the f/s interface have no impact on growth rate The optimized values of parameters with low sensitivity are not physically meaningful. Since only a single experimental curve was available to estimate nine parameters, at best only the most sensitive parameters, ΔG_1° and $D_{V_{\ddot{O}}}$, have been estimated in a meaningful manner. In fact, Equation 12 can be rewritten as

$$\frac{dx}{dt} = \frac{[P_1 + P_2 e^{-x/x_d}]}{x}, \qquad [13]$$

Table I. Parameter values and constants employed in the simulation of experimental data for Alloy 690 in high temperature water[20] using oxygen vacancies only (Figure 3a).

parameters / constants	value	unit
q_{Vo}	+2	
D_{Vo}	$2.61.10^{-23}$	m^2/s
$\phi_f(d_i)$	0.1	V
ΔV	0.01	V
α	0.5	
$\phi_{m/f}$	0.001	V
$\phi_{f/s}^\circ$	0.3	V
ΔG_1°	−15000	J/mol
ΔG_8°	−100000	J/mol
χ_{Cr}	0.32	
x_d	$5.0.10^{-8}$	

where P_1 and P_2 are lumped parameters given by

$$P_1 = K_1[\phi_f(x_i) + \Delta V]$$

$$P_2 = -K_1 \Delta V \alpha.$$

Consequently, a single thickness measurement can be used to estimate two parameters (for a given decay length); all the other parameter values cannot be determined by optimisation. All that can be said with confidence is that the fits in Figure 3 may be achieved with certain parameter values P_1 and P_2. For the simulation in Figure 3a, $P_1 = 3.9 \cdot 10^{-22}$ m^2/s and $P_2 = -1.8 \cdot 10^{-23}$ m^2/s .In Figure 3b, $P_1 = 8.0 \cdot 10^{-22}$ m^2/s and $P_2 = -3.6 \cdot 10^{-23}$ m^2/s. Given a set of operating conditions, the simplified model, Equation 13, can reproduce thickness versus time measurements by estimating only two parameters, which are functions of these operating conditions.

Model simplification (cations).— Equation 4 shows that M_{Cr} and I_{Cr} current densities have the same mathematical form as $J_{V_{\ddot{O}}}$. They can therefore be simplified in the same way to give expressions analogous to Equation 13. For $j = I_{Cr}$, $C_j^{m/f}/C_j^{f/s} \geq 1$ in Equation 11, so that, as for $J_{V_{\ddot{O}}}$, it is only necessary to satisfy $e^C > 50$, and thus, $\phi_f(x_i) > 0.1$ V, in order to obtain an equation analogous to Equation 13. For $j = M_{Cr}$, $C_j^{m/f}/C_j^{f/s} < 1$. In order to simplify Equation 11, it is in this case necessary to satisfy the condition $e^C \cdot C_j^{m/f}/C_j^{f/s} \gg 1$. This is the case for the practical parameter values used in all simulations here presented. It should be remembered that these conditions guarantee equivalence of the complete and simplified models, but even if

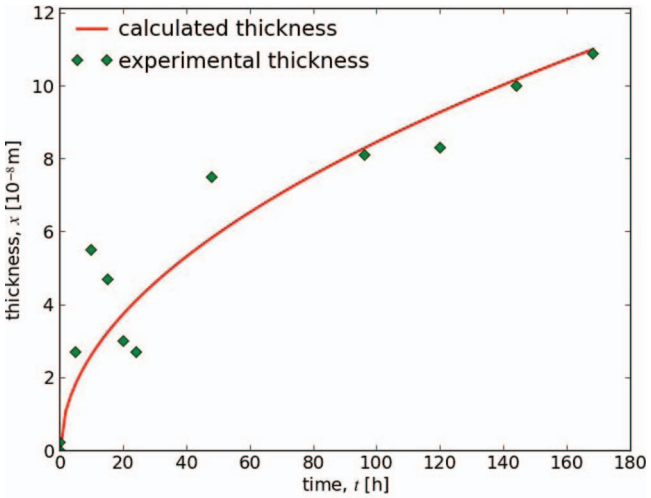

Figure 4. Experimental[21] and calculated film thickness using optimized parameters. $T = 573$ K, $pH = 10$ and $\chi_{Cr} = 0.19$.

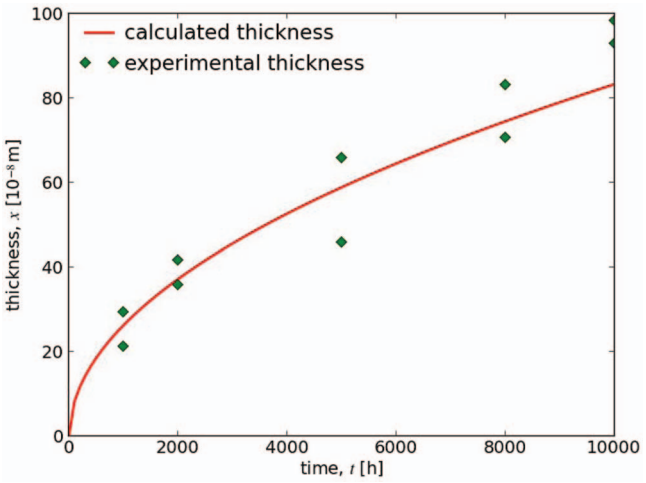

Figure 5. Experimental[22] and calculated film thickness using optimized parameters. $T = 533$ K, $pH = 6.7$ and $\chi_{Cr} = 0.19$.

they are not satisfied, the models may be equivalent or at least approximately so and the simulations show that the difference between the full and simplified models is indeed negligible.

From these simplifications, it follows that the growth rate is a sum of terms analogous to Equation 13,

$$\frac{dx}{dt} = \frac{[P_1 + P_2 e^{-x/x_d}]}{x} + \frac{[P_3 + P_4 e^{-x/x_d}]}{x} + \frac{[P_5 + P_6 e^{-x/x_d}]}{x}, \quad [14]$$

where

$$P_3 = \frac{q_{M_{Cr}} D_{M_{Cr}} \mathrm{F}}{RT} C^{m/f}_{M_{Cr}} [\phi_f(x_i) + \Delta V];$$

$$P_4 = -\frac{q_{M_{Cr}} D_{M_{Cr}} \mathrm{F}}{RT} C^{m/f}_{M_{Cr}} \Delta V \alpha;$$

$$P_5 = \frac{q_{I_{Cr}} D_{I_{Cr}} \mathrm{F}}{RT} C^{m/f}_{I_{Cr}} [\phi_f(x_i) + \Delta V];$$

$$P_6 = -\frac{q_{I_{Cr}} D_{I_{Cr}} \mathrm{F}}{RT} C^{m/f}_{I_{Cr}} \Delta V \alpha.$$

The six lumped parameters assume the following values for the simulation in Figure 7: $P_1 = 8.0 \cdot 10^{-22}$ m^2/s and $P_2 = -3.6 \cdot 10^{-23}$ m^2/s,

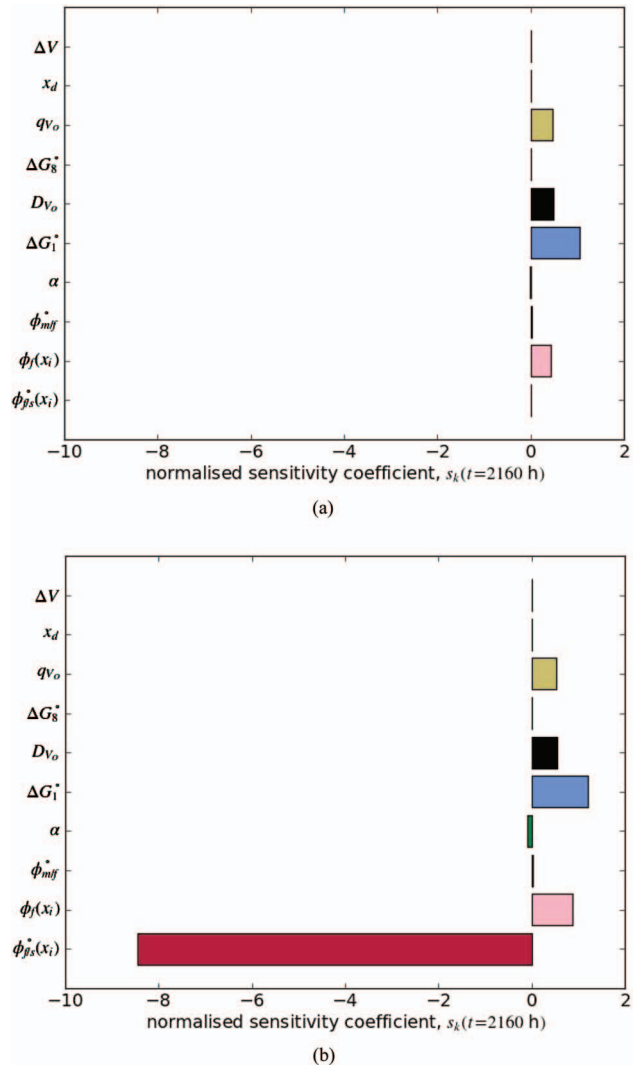

Figure 6. Normalized sensitivity coefficients of the optimized parameters at t = 2160 h, in the operating conditions of.[20] (a) Simulation using $J_{V_{\ddot{O}}}$ only (b) Simulation using all growth and dissolution fluxes.

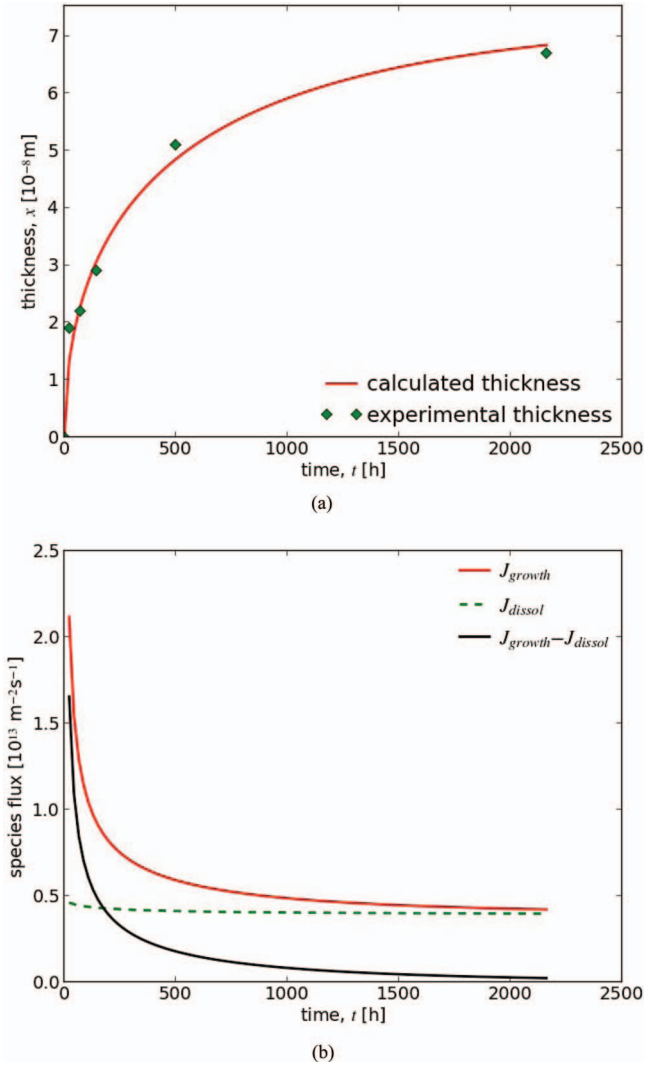

Figure 7. Experimental[20] and simulated film thickness and diffusional rates for Alloy 690 in high temperature water using optimized parameters for all J_{growth} and J_{dissol}. $T = 603$ *K*, $pH = 7.2$ and $\chi_{Cr} = 0.32$. (a) Film thickness (b) Growth and dissolution rates.

$P_3 = 6.1 \cdot 10^{-22}$ m^2/s, $P_4 = -2.8 \cdot 10^{-23}$ m^2/s, $P_5 = 8.5 \cdot 10^{-26}$ m^2/s and $P_6 = -3.9 \cdot 10^{-27}$ m^2/s. Part One of this study[9] showed how to calculate the concentrations $C^{m/f}_{M_{Cr}}$ and $C^{m/f}_{I_{Cr}}$; the respective expressions are given in Figure 5 of Part One.[9] Note that the dimensionless $C_{tot}|_M$ and $C_{tot}|_I$ are calculated from the unit cell of the oxide, taken to be hexagonal, of volume 289.52 Å^3 and containing 12 Cr^{3+} ions and 6 free interstitial sites, based on the assumption of a pure Cr_2O_3 layer:

$$C_{tot}|_M = \frac{12\Omega}{289.52 \cdot 10^{-30} N_V} = 2.89 \cdot 10^2$$

$$C_{tot}|_I = \frac{6\Omega}{289.52 \cdot 10^{-30} N_V} = 1.49 \cdot 10^2$$

$C_{Ni^{2+}(aq)}$ and $C_{Fe^{3+}(aq)}$ in Figure 5 of Part One[9] are the dimensionless concentrations of nickel and iron ions in the solution. According to the hypotheses made in Part One, these ions are the result of direct release from the alloy, since there is no iron or nickel in the oxide layer. As such, the concentrations are functions of time, and we are currently studying the possibility of modeling ion release so as to couple it with the oxide growth model. At present, the concentrations of ions in the solution are simply calculated as follows. The number of chromium atoms per unit of oxide in the layer is

$$C_{Cr} = \frac{2\rho_{Cr_2O_3}\Omega}{M_{Cr_2O_3}},$$

where $\rho_{Cr_2O_3}$ is the density of the oxide and $M_{Cr_2O_3}$ its molar mass. A simple proportionality then yields the aqueous concentrations of nickel and iron:

$$C_{Ni^{2+}(aq)} = \frac{\chi_{Ni}}{\chi_{Cr}} \frac{2\rho_{Cr_2O_3}\Omega}{M_{Cr_2O_3}}$$

$$C_{Fe^{3+}(aq)} = \frac{\chi_{Fe}}{\chi_{Cr}} \frac{2\rho_{Cr_2O_3}\Omega}{M_{Cr_2O_3}}.$$

Note that there are limits to the relative values that can be assumed by some of the parameters due to the fact that $C_{M_{Cr}}$ (in Figure 6 of Part One) must stay positive; this means that the values of P_3 and P_4 cannot assume all possible values.

Equation 14 can be simplified further and since its parameters are additive, one obtains again an expression similar to Equation 13,

$$\frac{dx}{dt} = \frac{[P + Qe^{-x/x_d}]}{x}, \qquad [15]$$

where $P = P_1 + P_3 + P_5$ and $Q = P_2 + P_4 + P_6$. For the result in Figure 7, $P = 1.4 \cdot 10^{-21}$ m^2/s, $Q = -6.4 \cdot 10^{-23}$ m^2/s. The same asymptotic behaviors discussed earlier for $J_{V_{\ddot{O}}}$ are equally applicable when all species are considered (Equation 15). Thus, thin films grow according to the parabolic law $x(t) = \sqrt{[P + Q]\, t}$ and thick films according to the (also parabolic) law $x(t) = \sqrt{P\, t}$.

The difficulty of determining physically meaningful parameters would have been increased considerably by addition of $J_{M_{Cr}}$ and $J_{I_{Cr}}$, as they introduce a number of free energies and diffusivities (Figure 5 of Part One). However, the above simplification is more convenient, as it allows one to capture growth kinetics using only two condition-dependent parameters. Furthermore, the fact that the diffusional rates of all of the species can be reduced to the same expression, supports the idea that a single species may be sufficient to model film growth as done in some previous studies.[6] Nevertheless, one would expect oxygen and/or cation vacancies to contribute the greater part to film growth and diffusion of cations to be less significant via interstitial sites, because of steric hindrance. Figure 8 shows the results of a simulation which partially supports this expectation, since $J_{I_{Cr}}$ is much smaller than $J_{V_{\ddot{O}}}$ and $J_{M_{Cr}}$ is of the same order of magnitude as $J_{V_{\ddot{O}}}$. This result was obtained using the parameters in Table II.

Film dissolution.— As discussed in an earlier section, a dissolution reaction is necessary to reproduce the pseudo-steady state plateau

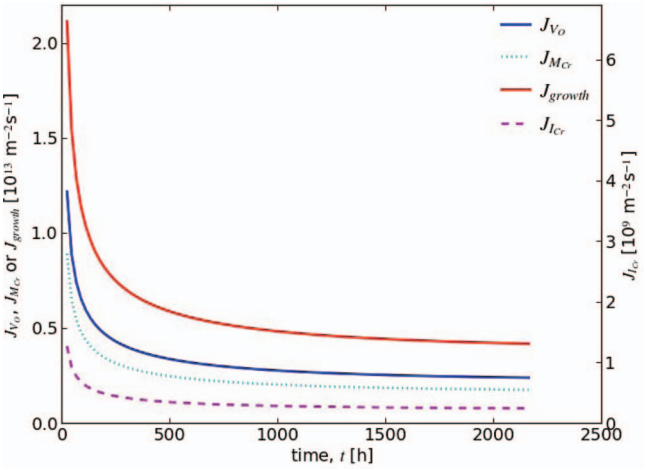

Figure 8. Diffusional rates of point defects contributing to film growth. $T = 603$ K, $pH = 7.2$ and $\chi_{Cr} = 0.32$.

generally observed in thickness measurements. Oxide films dissolve at the f/s interface due to the action of a non-conservative dissolution reaction. This process is generally held responsible for the level observed in many experimental thickness data. The rate of dissolution can be calculated according to the Arrhenius law of the reaction, $MO_{n/2} + nH^+ \rightleftarrows M^{\delta+}_{(aq)} + n/2\, H_2O + (\delta - n)e^-$, where the activation energy is modified by subtracting the potential drop $\phi_{f/s}$ from E_A:[12,9]

$$J_{diss} = k^\circ \exp\left[-\left(\frac{E_A}{kN_vT} - \frac{neN_v\phi_{f/s}(x)}{kN_vT}\right)\right][H^+]^m \qquad [16]$$

where $[H^+]^m = \exp(-2.303pH)^m$. Macdonald et al.[12] use this expression for dissolution, but consider $\phi_{f/s}$ constant with respect to x. In the more general model presented in[9] and used here, it is a function of x and consequently the rate of dissolution also becomes a function of x (and therefore of time). Interestingly, the strength of this dependence will depend on the value of the ratio $E_A/\phi_{f/s}$. When $E_A/\phi_{f/s} \gg 2.89 \cdot 10^5$ J $\cdot$ V^{-1}mol^{-1}, dissolution can be considered constant with respect to x. The shape of the curves in Figure 8 (species flux vs. time) makes it clear that dissolution must be constant in time, at least at the later times, if a steady state with a constant oxide film thickness is to be achieved, although it may possibly be a weak function of x at the beginning of the experiment. A simulation using the parameters in Table II allows for an excellent fit of thickness measurements as shown in Figure 7a for the data reported by Carrette.[20] It also shows that the best fit is achieved with a slight dependency of dissolution on x, given that $E_A/\phi_{f/s} = 1.83 \cdot 10^5$ J $\cdot$ V^{-1}mol^{-1}. Figure 7b shows that the overall growth rate, (here in the units of a current density, m^{-2}s^{-1}) given by the difference of J_{growth} and dissolution, is zero at steady state because $J_{growth} = J_{dissol}$. Note also that the sensitivity of $\phi^\circ_{f/s}$ in Figure 6b is not zero anymore, as the parameters relative to the f/s interface become non negligible compared to Figure 6a, when dissolution is introduced.

Like the growth rates, the dissolution rate can also be simplified by lumping parameters. Substituting $\phi^\circ_{f/s} + \Delta V \alpha e^{-x/x_d}$ for $\phi_{f/s}(x)$, Equation 16 can be rewritten as

$$J_{diss} = \mathrm{Re}^{Se^{-x/x_d}}, \qquad [17]$$

where

$$R = k^\circ e^{-2.303pH \cdot m} \exp\left[\frac{-E_A}{kN_vT} + \frac{ne}{kT}\phi^\circ_{f/s}\right]$$

$$S = \frac{ne}{kT}\Delta V \alpha$$

By subtracting the lumped dissolution rate law (Equation 17) from the lumped growth law (Equation 15), one obtains the overall rate of film

Table II. Parameter values and constants employed in the simulation of experimental data for Alloy 690 in high temperature water[20] using all the species contributing to growth and dissolution (Figures 6b, 7, 8).

parameters / constants	value	unit
q_{Vo}	+2	
D_{Vo}	$5.30.10^{-23}$	m^2/s
$\phi_f(d_i)$	0.1	V
ΔV	0.01	V
α	0.5	
$\phi_{m/f}$	0.001	V
$\phi_{f/s}^{\circ}$	0.3	V
ΔG_1°	−15000	J/mol
ΔG_8°	−100000	J/mol
χ_{Cr}	0.32	
χ_{Fe}	0.10	
χ_{Ni}	0.58	
n	3	
k°	$8.40.10^{16}$	$m^{-2}s^{-1}$
m	1	
E_a	54000	J/mol
D_{MCr}	$5.0.10^{-24}$	m^2/s
D_{ICr}	$1.0.10^{-20}$	m^2/s
ΔG_2°	−90000	J/mol
ΔG_4°	−30000	J/mol
ΔG_6°	−85000	J/mol
ΔG_9°	100000	J/mol
ΔG_{11}°	30000	J/mol
ΔG_{13}°	10000	J/mol
ΔG_{10}°	−1000	J/mol
ΔG_{12}°	−6000	J/mol
ΔG_{14}°	−3000	J/mol
ΔG_3°	85000	J/mol
ΔG_5°	10000	J/mol
ΔG_7°	10000	J/mol

growth and pseudo-steady state ($dx/dt = 0$) is attained when x exists such that the two terms on the right hand side equal each other:

$$\frac{dx}{dt} = \frac{[P + Qe^{-x/x_d}]}{x} - \mathrm{Re}^{Se^{-x/x_d}}.$$

Conclusions

A transient model for the growth kinetics of passive films on metals and alloys has been developed and the results of the numerical simulation have been compared to experimental film thickness measurements. Agreement is good and allows for estimation of model parameters. The main features distinguishing this model from previous descriptions of oxide film growth are

1) Its time-variant treatment of the electric field in the film and the potential differences over the film and the film solution interface
2) Inclusion of reactions involving all major alloy components (e.g. Cr, Ni, Fe)
3) Contribution of oxygen vacancies, cation vacancies and cations in interstitial positions to oxide growth. A pseudo-steady state can be reached when dissolution equals growth rate

Because it takes into account these often neglected aspects, the new model contains numerous parameters whose values are unknown. It can however be simplified significantly and parameters determined numerically. The simplified rate law makes it possible to analyze model behavior and draw some key conclusions:

1) In general the oxide growth rate law cannot be integrated analytically, so that the kinetics are neither logarithmic, inverse logarithmic nor parabolic. However both very thin and very thick films grow according to parabolic laws. These behaviors are a direct result of the transient evolution of the potential drop in the film. The period of transient evolution is started when an external environmental input (such as a change in temperature) disturbs the alloy-film-solution system. In absence of such an input, the system is at steady state and the growth rate follows a constant square root law.
2) The sum of all the species diffusional rates contributing to film growth can be expressed through a law of the type

$$J_{growth} = \frac{[P + Qe^{-x/x_d}]}{x},$$

where P and Q are lumped parameters which enclose the contributions of all the species (anionic vacancies, cationic vacancies, cation interstitials). It is thus not surprising that previous growth models have been able to fit experimental data though hypothesizing a single contributing species.
3) Film dissolution rate is in general a function of time during transient film growth.

List of Symbols

F	Faraday's constant (96484.6 C / mol)
R	universal gas constant (8.31441 J / mol / K)
k	Boltzmann's constant ($1.38.10^{-23}$ J / K)
T	temperature (K)
Ω	molar volume of the oxide ($2.92.10^{-5}$ m^3 / mol)
χ_{Cr}	mole fraction of Cr in the alloy
χ_{Fe}	mole fraction of Fe in the alloy
χ_{Ni}	mole fraction of Ni in the alloy
$\phi_{m/f}$	potential drop at the metal/oxide interface (V)
$\phi_{f/s}$	potential drop at the oxide/electrolyte interface (V)
ϕ_f	potential drop inside the oxide film (V)
x	oxide film thickness (m)
d	distance/ position (m)
x_i	initial oxide thickness (m)
x_f	final (steady state) oxide thickness (m)
x_d	decay length (m)
F	electric field in the oxide layer (V / m)
V	total potential drop in the metal/oxide/electrolyte system (V)
ΔV	potential variation (V)
C_j	concentration of species j (number of species / m^3)
D_j	diffusion coefficient of charged species j (m^2 / s)
ΔG_p°	Gibbs free energy of reaction p (J/mol)
J_j	flux of species j (number of species per unit area per unit time)
q_j	charge of species j
M_{Cr}	chromium cation in a lattice position in the oxide
$V_{\ddot{O}}$	oxygen vacancy in the oxide
I_{Cr}	chromium cation in an interstitial position in the oxide
k°	pre-exponential factor of the dissolution reaction ($m^{-2}s^{-1}$)
E_a	activation energy of the dissolution reaction (J/mol)
m	reaction order of the dissolution reaction with respect to H^+ ions
ρ_{Cr2O3}	oxide density (kg / m^3)
M_{Cr2O3}	oxide molar mass

References

1. I. Olefjord, *Materials Science & Engineering*, **42**, 161 (1980).
2. H.-H. Strehblow, V. Maurice, and P. Marcus, *Corrosion Mechanisms in Theory and Practice*. CRC Press, 2011, ch. 5.
3. C. Wagner, *Zeitschrift für Physikalische Chemie*, **B41**, 42 (1933).
4. N. F. Mott, *Transactions of the Faraday Society*, **35**, 1175 (1939).
5. F. P. Fehlner and N. F. Mott, *Oxid. Met.*, **2**, 59 (1970).
6. C. Chao, L. Lin, and D. Macdonald, *J. Electrochem. Soc.*, **128**, 1187 (1981).
7. M. Bojinov, *J. Solid State Electrochem.*, **1**, 161 (1997).
8. B. Diawara, Y. Beh, and P. Marcus, *J. Phys. Chem. C*, **114**, 19299 (2010).

9. A. Seyeux, B. Diawara, V. Maurice, and P. Marcus, Submitted to *J. Electrochem. Soc.*
10. N. F. Mott, *Trans. Faraday Soc.*, **43**, 429 (1947).
11. N. Cabrera, *Rep. Prog. Phys.*, **12**, 163 (1949).
12. D. D. Macdonald and M. Urquidi-Macdonald, *J. Electrochem. Soc.*, **137**, 2395 (1990).
13. L. Zhang and D. D. Macdonald, *Electrochim. Acta*, **43**, 679 (1998).
14. D. D. Macdonald, *Electrochim. Acta*, **56**, 1761 (2011).
15. L. Zhang, D. D. Macdonald, E. Sikora, and J. Sikora, *J. Electrochem. Soc.*, **145**(3), 898 (1998).
16. B. Krishnamurthy, R. E. White, and H. J. Ploehn, *Electrochim. Acta*, **46**, 3387 (2001).
17. B. Beverskog, M. Bojinov, P. Kinnunen, T. Laitinen, K. Mäkelä, and T. Saario, *Corros. Sci.*, **44**, 1923 (2002).
18. http://www.themai.org/.
19. http://www.salome-platform.org/about/yacs.
20. F. Carrette, Ph.D. dissertation, Institut National Polytechnique de Toulouse, 2002.
21. R. L. Tapping, R. D. Davidson, E. McAlpine, and D. H. Lister, *Corros. Sci.*, **26**, 563 (1986).
22. S. E. Ziemniak and M. Hanson, *Corros. Sci.*, **44**, 2209 (2002).